Quantized Superfluid Vortex Rings in the Unitary Fermi Gas

Aurel Bulgac,[1] Michael McNeil Forbes,[2,1,3] Michelle M. Kelley,[4] Kenneth J. Roche,[5,1] and Gabriel Wlazłowski[6,1]
[1]*Department of Physics, University of Washington, Seattle, Washington 98195-1560, USA*
[2]*Institute for Nuclear Theory, University of Washington, Seattle, Washington 98195-1550, USA*
[3]*Department of Physics and Astronomy, Washington State University, Pullman, Washington 99164-2814, USA*
[4]*Department of Physics, University of Illinois at Urbana-Champaign, Il 61801-3080, USA*
[5]*Pacific Northwest National Laboratory, Richland, Washington 99352, USA*
[6]*Faculty of Physics, Warsaw University of Technology, Ulica Koszykowa 75, 00-662 Warsaw, Poland*
(Received 20 June 2013; published 16 January 2014)

In a recent article, Yefsah *et al.* [Nature (London) **499**, 426 (2013)] report the observation of an unusual excitation in an elongated harmonically trapped unitary Fermi gas. After phase imprinting a domain wall, they observe oscillations almost an order of magnitude slower than predicted by any theory of domain walls which they interpret as a "heavy soliton" of inertial mass some 200 times larger than the free fermion mass or 50 times larger than expected for a domain wall. We present compelling evidence that this "soliton" is instead a quantized vortex ring, by showing that the main aspects of the experiment can be naturally explained within the framework of time-dependent superfluid density functional theories.

DOI: 10.1103/PhysRevLett.112.025301 PACS numbers: 67.85.Lm, 03.75.Kk, 03.75.Ss, 67.85.De

Collective modes in the form of topological and dynamical defects—solitons, vortices, vortex rings, etc.—embody the emergence of nontrivial collective dynamics from microscopic degrees of freedom, and provide a challenge for many-body theories from cold atoms through electronic superconductors to nuclei and neutron stars. The unitary Fermi gas (UFG) provides an ideal strongly interacting system for measuring and testing collective modes where controlled experiments and theoretical techniques are starting to converge [1]. A handful of predicted collective modes have been directly observed, including collective oscillations of harmonically trapped gases [2,3], higher-nodal collective modes [4], scissor modes [2], quantized vortices and vortex lattices [5], shock waves [6], and phonons (speed of sound [7], critical velocity [8], and first and second sound [4,9]). Other modes, such as the Higgs mode [10,11], vortex rings [12], and domain walls [13–17], have been demonstrated in simulations, but await direct observation. In this Letter, we discuss the objects observed in [18]: they interpret these as "heavy solitons"; we show them to be vortex rings.

Experimental puzzle: Slowly moving "solitons."—The recent MIT experiment [18] measures a slowly moving soliton produced by a sharp spatially delineated phase imprint on an ultracold cloud of some 10^5 ^{6}Li atoms in an elongated harmonic trap. These solitons cannot be resolved *in situ*, but appear after a specific time-of-flight expansion procedure that includes a rapid ramp of the interaction strength which is controlled through a Feshbach resonance by an external magnetic field. In particular, they note that a certain minimum field $B_{\min} < 700$ G is required to resolve the solitons (discussed in their Supplemental Material). From the images, they extract the period of oscillation, and find that it increases as the inverse trap aspect ratio $1/\lambda$ and the magnetic field B are increased. Increasing the temperature, they observe "antidampening" whereby the amplitude of the oscillation increases with time. The authors interpret these results as the observation of a heavy soliton with a mass "more than 50 times larger than the theoretically predicted value" and "200 times their bare mass."

Topological objects in the BEC-BCS crossover.—Superfluids are characterized by a complex-valued order parameter Ψ that describes the condensate wave function in Bose-Einstein condensates (BECs) and the Cooper pair condensate in fermionic Bardeen-Cooper-Schrieffer (BCS) superfluids. The superfluid ground state picks a coherence overall phase of the complex order parameter, spontaneously breaking the original $U(1)$ phase symmetry of the theory. Sound waves manifest as fluctuations in this coherent phase (phonons or Nambu-Goldstone modes). Landau's original argument for ^{4}He superfluidity posits a kinematical critical flow velocity v_c below which neither pair-breaking nor sound excitations can be generated. This argument is spoiled by the generation of topologically stable excitations that can nucleate at the edge of the fluid, lowering the v_c. The dynamics of these topological excitations and their interactions are at the heart of quantum turbulence studies [19].

The single-valued order parameter admits several topologically stable objects in three dimensions. Domain walls separate regions of different phases while vortices correspond to the phase winding around a line along which the order parameter vanishes. In bosonic theories (BEC limit), the number density $n \propto |\Psi|^2$ vanishes in the core of vortices and in stationary domain walls, giving these objects a "negative mass. For fermions, while the complex order parameter has a similar behavior, the relationship $n \propto |\Psi|^2$ breaks down, with the interpretation that the core of the topological defects are filled with "normal" fluid, but

 © 2014 American Physical Society

at unitarity the number density depletion is still substantial [12,20,21]. A manifestation of this negative mass is that the amplitude of oscillation in a trap will increase as energy is lost. This antidamping is seen in the experiment [18].

Domain walls (often referred to as solitons) are topologically stable in one dimension. Their thickness is set by the coherence length $l_{\rm coh}$ and thus they have a negative effective mass ($-M_{\rm DW}$) due to the density depletion $M_{\rm DW} = mN_{\rm DW}$, where $N_{\rm DW} \sim n\pi R^2 l_{\rm coh}$ is the depletion for a gas cloud of number density n in a trap of radius R. In the unitary limit, all scales are set by the Fermi wave vector k_F with $n = k_F^3/3\pi^2$ and $l_{\rm coh} \sim k_F^{-1}$ and thus, $M_{\rm DW} \sim k_F^2 R^2 m$ is much larger than the mass m of a single fermion. In quantum mechanics, the dynamics of heavy objects is generally well approximated by classical equations of motion. For domain walls, both kinetic and potential energies are localized on the wall; thus, the same mass $M_{\rm DW}$ enters both the kinetic and potential terms and one expects the oscillation period T to be comparable to the natural axial period T_z of the trapping potential. This is confirmed in BEC experiments [22] where $T \approx \sqrt{2}T_z$ and by fermionic simulations [13], where $T \approx \sqrt{3}T_z$.

In contrast, vortex rings [23], which also occur in classical fluids [24], have very different dynamics. In infinite media, for example, with logarithmic accuracy, large rings ($R \gg l_{\rm coh} \sim k_F^{-1}$) have linear momentum $p \sim mn\kappa\pi R^2$, dispersion $\varepsilon(p)$, and speed $v = {\rm d}\varepsilon(p)/{\rm d}p$ [25]

$$\varepsilon \sim \frac{mn\kappa^2 R}{2} \ln \frac{R}{l_{\rm coh}}, \qquad v \sim \frac{\kappa}{4\pi R} \ln \frac{R}{l_{\rm coh}}, \tag{1a}$$

where κ is the circulation. Their speed $v \propto \ln p/\sqrt{p}$ thus *decreases* as the momentum, kinetic energy, and radius increase. Unlike for domain walls, their inertial mass $M_I = F/\dot{v} \sim mn\kappa 8\pi^2 R^3/\ln(R/l_{\rm coh})$, (where $F = \dot{p}$ is the force), differs from the effective mass due to the density depletion $M_{\rm VR} = mN_{\rm VR} \sim mn2\pi^2 R l_{\rm coh}^2$ and the period of oscillation can receive a significant enhancement

$$\frac{T}{T_z} \sim \sqrt{\frac{M_I}{M_{\rm VR}}} \sim \frac{2R/l_{\rm coh}}{\sqrt{\ln(R/l_{\rm coh})}}. \tag{1b}$$

This estimate (1b) gives only an order of magnitude estimate: the dynamics of a vortex ring in a finite trap is somewhat more complicated but can be qualitatively understood. Each element of the ring will experience an outward buoyant force $\boldsymbol{F}_B \approx N_{\rm VR}\nabla V_{\rm trap}$, where $V_{\rm trap} = m\omega_\perp^2(x^2 + y^2 + z^2/\lambda^2)/2$ (with $\lambda > 1$). The Magnus relationship $\boldsymbol{F}_B = mn(\boldsymbol{v} - \boldsymbol{v}_s) \times \boldsymbol{\kappa}$ will thus adjust the velocity $\boldsymbol{v}$ with two components: one counter to $\boldsymbol{v}_s$ and another that causes the ring to expand and contract near the ends of the trap. The velocity $\boldsymbol{v}_s$ is the superflow induced by the phase winding of the rest of the vortex ring on the element, and is parallel to the z axis of the trap. In the middle of the trap $z \approx 0$, small rings (R much less than the trap waist $R_\perp$) will experience little buoyant force and the motion will be dominated by $\boldsymbol{v} \approx \boldsymbol{v}_s$. Larger rings, however, will have a smaller $\boldsymbol{v}_s$ and larger $\boldsymbol{F}_B$: at a critical radius R_c, the Magnus effect will cancel $\boldsymbol{v}_s$ and the ring will remain stationary. Larger rings $R > R_c$ will crawl backwards along the trap. Near the ends of the trap, the buoyant force will also cause the rings to expand at one end and contract at the other. Thus a vortex ring may oscillate along the trap as observed in bosons [26].

Heavy solitons are indeed vortex rings.—While a quantitative discussion requires a more complete analysis along the lines of [27] or direct simulation as we shall present in a moment, the order of magnitude of the effect can be estimated from Eq. (1b) which is approximately valid for small vortex rings near the middle of the trap $z \approx 0$. For the experimental parameters, small rings $R \approx 0.2R_\perp$ (rings with this radius have roughly the same amplitude as the oscillations seen in the experiment) exhibit periods an order of magnitude larger than T_z, naturally explaining the observations. Furthermore, as the system is brought into the BEC regime, the coherence length $l_{\rm coh}$ will grow significantly relative to the fixed ring size R, so T will naturally get smaller, approaching T_z. Finally, in the extreme BEC limit, $l_{\rm coh}$ will approach the width of the trap, arresting the snake instability, and reproducing the theoretical prediction $T \approx \sqrt{2}T_z$ for a domain wall.

Method.—To explain more subtle features of the experiment, like the observed dependence on aspect ratio, we perform dynamical simulations of trapped unitary fermions using two formulations of density functional theory (DFT). The first, an extended Thomas-Fermi (ETF) model [28], is essentially a bosonic theory for the dimer or Cooper-pair wave function Ψ. The dynamics are described by a nonlinear Schrödinger equation (NLSEQ) similar to the Gross-Pitaevskii equation (GPE) for bosons

$$i\hbar\frac{\partial\Psi}{\partial t} = -\frac{\hbar^2}{4m}\nabla^2\Psi + 2\frac{\partial\mathcal{E}_h(n,a)}{\partial n}\Psi + 2V_{\rm ext}\Psi, \tag{2}$$

where arguments $\boldsymbol{x}$ and t have been suppressed, $n = 2|\Psi|^2$ is the fermion number density, and $\mathcal{E}_h(n,a)$ is the energy-density of the homogeneous gas with density n and (adjustable) scattering length a fit to the equation of state in the BEC-BCS crossover. This simplified DFT is equivalent to zero-temperature quantum hydrodynamics (including the so-called quantum pressure term), and we shall use this to model the time-of-flight expansion and imaging procedure of the experiment. While computationally attractive, this formulation has some physical drawbacks. In particular, it models only the superfluid portion of the cloud: physics associated with the normal state is missing. As a result, a vanishing order parameter $\Psi = 0$ implies a vanishing density $n = 0$. This tends to overestimate the density contrast in the core of defects and leads to the same domain wall motion $T \approx \sqrt{2}T_z$ as the harmonically trapped GPE.

There is also no mechanism for the superfluid to transfer energy to the normal component, which inhibits the relaxation of rotating systems into a regular vortex lattice, and prevents Eq. (2) from being used to simulate the preparation of the experiment as the initial sound waves generated by the phase imprint never dampen, and the generated vortex rings rapidly decay.

To address these issues, we also simulate a time-dependent extension of DFT to superfluid systems—the time-dependent superfluid local density approximation (TDSLDA)—where the dynamical evolution is described by equations for the quasiparticle wave functions (u_k, v_k)

$$i\hbar\frac{\partial}{\partial t}\begin{pmatrix} u_k \\ v_k \end{pmatrix} = \begin{pmatrix} h & \Delta \\ \Delta^* & -h \end{pmatrix}\begin{pmatrix} u_k \\ v_k \end{pmatrix}, \tag{3a}$$

where $h = \delta\mathcal{E}/\delta n$ and $\Delta = \delta\mathcal{E}/\delta\nu^*$ (ν is the anomalous density) [29]. This is similar in form to the Bogoliubov–de Gennes (BdG) mean-field theory [13–16], but includes a self-energy contribution β and effective mass parameter α neglected in the BdG:

$$h = \frac{\delta\mathcal{E}}{\delta n} = \alpha\frac{-\hbar^2\nabla^2}{2m} + \beta\frac{(3\pi^2 n)^{2/3}}{2} - \frac{|\Delta|^2}{3\gamma n^{2/3}}. \tag{3b}$$

These additional terms allows the TDSLDA to quantitatively match all experimentally measured and numerically calculated properties of homogeneous systems in finite and infinite boxes [30]: adjusting α, β, and γ allows one to consistently characterize the energy per particle, pairing gap, and quasiparticle spectrum obtained from quantum Monte Carlo (QMC) calculations of the homogeneous infinite system. (Note: If $\alpha \neq 1$, one must include additional terms to restore Galilean covariance as discussed in [29,31]: we avoid this complication by setting $\alpha = 1$ instead of $\alpha \approx 1.1$ while adjusting β and γ to reproduce the energy per particle and pairing gap.) Simulating Eqs. (3) for three-dimensional systems represents a serious computational challenge that effectively utilizes the largest supercomputers available, so we use this only to verify that stable vortex rings are generically produced from the phase-imprint procedure, and use the ETF to illustrate the behavior of the experimental systems.

Results.—Following the preparation procedure outlined in [18], we phase imprint a domain wall on harmonically trapped clouds and follow the evolution using the TDSLDA. (Details are presented in [31].) For sufficiently large clouds, the domain wall quickly decays into an oscillating vortex ring. Figure 1 shows the motion as the ring initially crawls along the outside of the trap and a smaller ring bounces back. Computational limitations restrict us to relatively small systems and these simulations are quite close to the onset of the snake instability. Nevertheless, the period seen in Fig. 1 is comparable to our estimate Eq. (1b). Finally, we note an antidamping similar to that

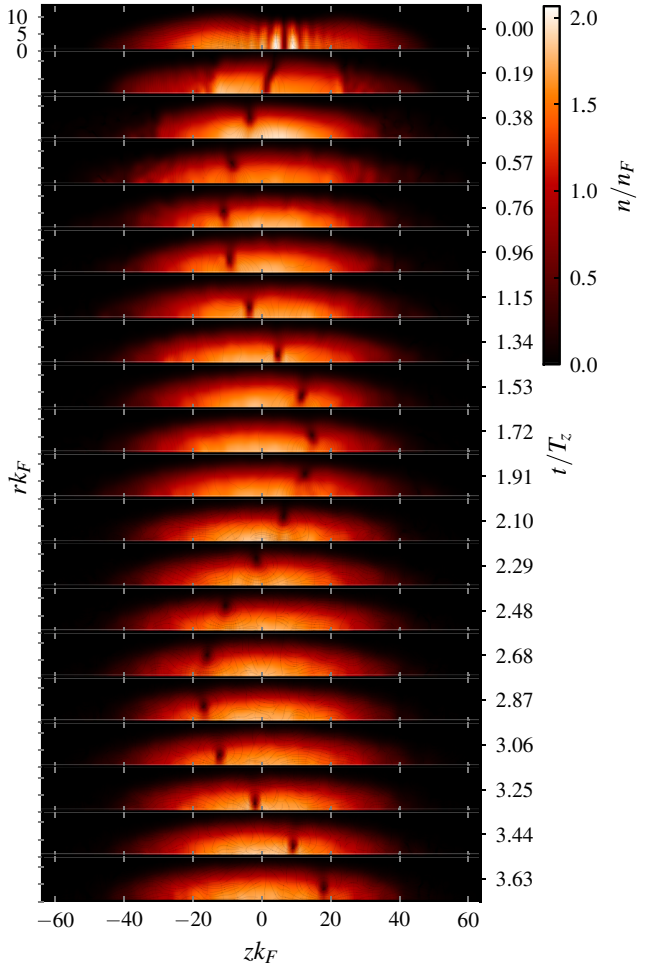

FIG. 1 (color online). Oscillations of a vortex ring in an elongated harmonic trap. Simulated with the TDSLDA on a $32 \times 32 \times 128$ lattice for a cloud with 560 particles. We evolve about 10^5 wave functions in real time using a symplectic split-operator integrator that respects time-reversal invariance using hundreds of GPUs on the Titan supercomputer [32]. More details and several movies may be found in [31].

seen at higher temperatures in [18]. This is explained by the small heat capacity of our simulated system: the residual sound waves induced by the phase correspond roughly to a finite temperature.

For larger clouds we use the ETF . As expected, the initial preparation phase cannot be reliably reproduced: the sound waves generated by the imprint do not dissipate, and the resulting vortex ring decays within a few oscillations. Stable vortex rings can be produced, however, by "cooling" an imprinted phase pattern with imaginary time evolution. As shown in the Supplemental Material [31], these vortex rings reproduce the qualitative behaviors observed in the MIT experiment [18]. In particular, the period is an order of magnitude larger than expected for domain walls and increases by similar amounts as the aspect ratio is reduced as shown in Table I. The period also scales toward the domain wall results $\sqrt{2}T_z$ toward the

TABLE I. Dependence of the oscillation period on aspect ratio for a vortex ring imprinted with $R_0 = 0.30R_\perp$ at resonance. Note that the ETF consistently underestimates the period by about a factor of 0.56.

Aspect ratio	ETF period	Observed period [18]
$\lambda = 3.3$	$T = 9.9T_z$	$T = 18(2)T_z$
$\lambda = 6.2$	$T = 8.4T_z$	$T = 14(2)T_z$
$\lambda = 15$	$T = 6.7T_z$	$T = 12(2)T_z$

BEC limit and exhibits antidamping decays in the presence of phonon excitations. (These phonons mock up fluctuations, but do not faithfully simulate a thermal ensemble.) A quantitative comparison is marred by the lack of a normal component occupying the core of the vortex. However, when comparing the ETF with the TDSLDA simulations, we find that this is fairly consistently characterized by an overall increase in periods by a factor of about 1.8—somewhat larger but similar to the factor of $\approx\sqrt{3/2}$ seen when comparing the period of fermionic to bosonic domain walls in quasi-1D environments. We are confident that a realistic TDSLDA simulation would closely mimic the experiment, and enforcing quantitative agreement would help further constrain the TDSLDA functional.

The puzzle provided by the imaging procedure remains: can a vortex ring look like a planar soliton after imaging? The answer, yes, is demonstrated in Fig. 2 and in [31]. The imaging procedure includes a rapid ramp of the magnetic field to the BEC side of the crossover where the coherence length becomes much larger, but the equation of state becomes softer. This rapid-ramp procedure followed by expansion produces something akin to a shock wave [6,17] that manifests itself as a planar soliton upon imaging. Our simulations confirm the somewhat subtle experimental observation that sufficient ramping below $B_{\min} < 700$ G is required to observe a signal, and explains both the thickness of the soliton and the amplitude of the integrated density fluctuations observed in the experiment [18]. A slight difference remains between the density fringe pattern seen in the integrated 1D density Fig. 2 compared with those seen in experiment [18], the latter having a minimum in the center where the ETF has a peak. As shown in the movies of the expansion [31], this feature results from the motion of shock waves formed during the expansion, the speed of which will be incorrectly predicted by the ETF.

We have shown that the puzzling report of heavy solitons in fermionic superfluids [18], which appear to exhibit an effective mass some 50 times larger than predicted by the theory of dynamics of a domain wall, can be naturally explained in terms of vortex rings. Using a 3D simulation of the TDSLDA, we validate the picture that, in large enough traps, imprinted domain walls generically evolve into vortex rings through an axially symmetric "snake instability. The estimate Eq. (1b) shows that these rings

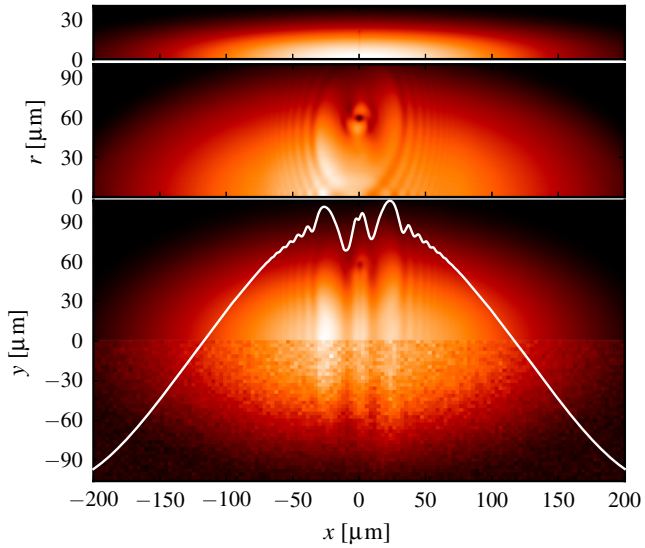

FIG. 2 (color online). Demonstration of the imaging procedure. The top plot shows a slice of the density through the upper-half core of the trap before expansion: the vortex ring is barely visible at $z = 0$. Below is a slice through the upper-half core after ramping to $B_{\min} = 580$ G and letting the cloud expand as discussed [18]. The lower plot shows the integrated 2D density $\int \mathrm{x}\, n(x, y, z)$ and the integrated 1D density $\int \mathrm{x}\, \mathrm{y}\, n(x, y, z)$ (white curve). The lower half of the image has added Gaussian noise with a 3% density variation and is coarse grained on a 3 μm scale to simulate the experimental imaging procedure, clearly demonstrating that vortex rings appear as solitons. (Densities are scaled by maximum value for better contrast.) For $B_{\min} > 700$ G , the density contrast is reduced below the experimental signal-to-noise ratio. See the Supplemental Material [31] for details and for movies.

can have large periods at unitarity, that decreases toward the BEC regime, and explicit simulations using the ETF verify the dependence of the period on the aspect ratio. Finally, the ETF demonstrates that, through the expansion and imaging process employed to resolve the objects, vortex rings manifest as large planar objects with an observable density contrast only if the magnetic field is ramped to $B_{\min} < 700$ G, in quantitative agreement with the observations. We have thus verified virtually all aspects of the experiment [18], including the elaborate imaging protocol, thereby validating the use of the TDSLDA and ETF theories for dynamical simulations including topological defects, and resolving the mystery of heavy solitons as vortex rings.

We acknowledge support under U.S. Department of Energy (DoE) Grants No. DE-FG02-97ER41014 and No. DE-FG02-00ER41132. M. M. K. acknowledges the support provided by an REU NSF fellowship. G. W. acknowledges the Polish Ministry of Science for the support under Contract No. N N202 128439, within the program "Mobility Plus-I edition" under Contract No. 628/MOB/2011/0, and the Polish National Science Center

(NCN) decision No. DEC-2013/08/A/ST3/00708. Some of the calculations reported here have been performed at the University of Washington Hyak cluster funded by the NSF MRI Grant No. PHY-0922770. This research also used resources of the National Center for Computational Sciences at Oak Ridge National Laboratory, which is supported by the Office of Science of the DOE under Contract No. DE-AC05-00OR22725. We thank R. Sharma and M. Zwierlein for discussions.

[1] *The BCS–BEC Crossover and the Unitary Fermi Gas*, edited by W. Zwerger, Lecture Notes in Physics Vol. 836 (Springer–Verlag, Berlin, Heidelberg, 2012).
[2] M. Bartenstein, A. Altmeyer, S. Riedl, S. Jochim, C. Chin, J. H. Denschlag, and R. Grimm, Phys. Rev. Lett. **92**, 203201 (2004); A. Altmeyer, S. Riedl, M. J. Wright, C. Kohstall, J. H. Denschlag, and R. Grimm, Phys. Rev. A **76**, 033610 (2007); M. J. Wright, S. Riedl, A. Altmeyer, C. Kohstall, E. R. Sánchez Guajardo, J. H. Denschlag, and R. Grimm, Phys. Rev. Lett. **99**, 150403 (2007); S. Riedl, E. R. Sánchez Guajardo, C. Kohstall, A. Altmeyer, M. J. Wright, J. H. Denschlag, R. Grimm, G. M. Bruun, and H. Smith, Phys. Rev. A**78**, 053609 (2008).
[3] J. Kinast, S. L. Hemmer, M. E. Gehm, A. Turlapov, and J. E. Thomas, Phys. Rev. Lett. **92**, 150402 (2004); J. Kinast, A. Turlapov, and J. E. Thomas, Phys. Rev. A **70**, 051401 (2004).
[4] E. R. S. Guajardo, M. K. Tey, L. A. Sidorenkov, and R. Grimm, Phys. Rev. A **87**, 063601 (2013).
[5] M. W. Zwierlein, J. R. Abo-Shaeer, A. Schirotzek, C. H. Schunck, and W. Ketterle, Nature (London) **435**, 1047 (2005).
[6] J. A. Joseph, J. E. Thomas, M. Kulkarni, and A. G. Abanov, Phys. Rev. Lett. **106**, 150401 (2011).
[7] J. Joseph, B. Clancy, L. Luo, J. Kinast, A. Turlapov, and J. E. Thomas, Phys. Rev. Lett. **98**, 170401 (2007).
[8] D. E. Miller, J. K. Chin, C. A. Stan, Y. Liu, W. Setiawan, C. Sanner, and W. Ketterle, Phys. Rev. Lett. **99**, 070402 (2007).
[9] M. K. Tey, L. A. Sidorenkov, E. R. Sánchez Guajardo, R. Grimm, M. J. H Ku, M. W. Zwierlein, Y.-H. Hou, L. Pitaevskii, and S. Stringari, Phys. Rev. Lett. **110**, 055303 (2013); L. A. Sidorenkov, M. K. Tey, R. Grimm, Y.-H. Hou, L. Pitaevskii, and S. Stringari, Nature (London) **498**, 78 (2013).
[10] A. Bulgac and S. Yoon, Phys. Rev. Lett. **102**, 085302 (2009).
[11] R. G. Scott, F. Dalfovo, L. P. Pitaevskii, and S. Stringari, Phys. Rev. A **86**, 053604 (2012).
[12] A. Bulgac, Y.-L. Luo, P. Magierski, K. J. Roche, and Y. Yu, Science **332**, 1288 (2011).
[13] R. G. Scott, F. Dalfovo, L. P. Pitaevskii, and S. Stringari, Phys. Rev. Lett. **106**, 185301 (2011).
[14] M. Antezza, F. Dalfovo, L. P. Pitaevskii, and S. Stringari, Phys. Rev. A **76**, 043610 (2007).
[15] A. Spuntarelli, L. D. Carr, P. Pieri, and G. C. Strinati, New J. Phys.**13**, 035010 (2011).
[16] R. Liao and J. Brand, Phys. Rev. A **83**, 041604 (2011).
[17] A. Bulgac, Y.-L. Luo, and K. J. Roche, Phys. Rev. Lett. **108**, 150401 (2012).
[18] T. Yefsah, A. T. Sommer, M. J. H Ku, L. W. Cheuk, W. Ji, W. S. Bakr, and M. W. Zwierlein, Nature (London) **499**, 426 (2013).
[19] W. F. Vinen and J. J. Niemela, J. Low Temp. Phys. **128**, 167 (2002); W. F. Vinen, J. Low Temp. Phys. **145**, 7 (2006); W. F. Vinen, J. Low Temp. Phys. **161**, 419 (2010); L. Skrbek, J. Phys. Conf. Ser. **318**, 012004 (2011); M. Tsubota, J. Phys. Soc. Jpn. **77**, 111006 (2008); M. Tsubota, M. Kobayashi, and H. Takeuchi, Phys. Rep. **522**, 191 (2013); M. S. Paoletti and D. P. Lathrop, Annu. Rev. Condens. Matter Phys. **2**, 213 (2011).
[20] A. Bulgac and Y. Yu, Phys. Rev. Lett. **91**, 190404 (2003).
[21] Y. Yu and A. Bulgac, Phys. Rev. Lett. **90**, 161101 (2003).
[22] C. Becker, S. Stellmer, P. Soltan-Panahi, S. Dorscher, M. Baumert, E.-M. Richter, J. Kronjager, K. Bongs, and K. Sengstock, Nat. Phys. **4**, 496 (2008); A. Weller, J. P. Ronzheimer, C. Gross, J. Esteve, M. K. Oberthaler, D. J. Frantzeskakis, G. Theocharis, and P. G. Kevrekidis, Phys. Rev. Lett. **101**, 130401 (2008).
[23] G. W. Rayfield and F. Reif, Phys. Rev. **136**, A1194 (1964).
[24] H. Lamb, *Hydrodynamics* (Dover, New York, 1945), 6th ed.; P. Saffman, *Vortex Dynamics* (Cambridge University Press, Cambridge, England, 1992).
[25] P. Roberts and R. Donnelly, Phys. Lett. **31A**, 137 (1970); C. F. Barenghi and R. J. Donnelly, Fluid Dyn. Res. **41**, 051401 (2009).
[26] I. Shomroni, E. Lahoud, S. Levy, and J. Steinhauer, Nat. Phys. **5**, 193 (2009).
[27] S. Komineas, Eur. Phys. J. Spec. Top. **147**, 133 (2007).
[28] Y. E. Kim and A. L. Zubarev, Phys. Lett. A **327**, 397 (2004); Y. E. Kim and A. L. Zubarev, Phys. Rev. A **70**, 033612 (2004); L. Salasnich, F. Ancilotto, N. Manini, and F. Toigo, Laser Phys. **19**, 636 (2009); L. Salasnich and F. Toigo, Phys. Rev. A **78**, 053626 (2008); L. Salasnich and F. Toigo, Phys. Rev. A **82**, 059902(E) (2010).
[29] A. Bulgac, M. M. Forbes, and P. Magierski, in *The BCS-BEC Crossover and the Unitary Fermi Gas*, edited by W. Zwerger, Lecture Notes in Physics Vol. 836 (Springer, New York, 2012), Chap. 9, p. 305; A. Bulgac, Annu. Rev. Nucl. Part. Sci. **63**, 97 (2013).
[30] M. M. Forbes, S. Gandolfi, and A. Gezerlis, Phys. Rev. A **86**, 053603 (2012).
[31] See Supplemental Material at http://link.aps.org/supplemental/10.1103/PhysRevLett.112.025301 for details about our numerical calculations, movies, and figures with finer resolution. Additional movies are available at: http://www.phys.washington.edu/~bulgac/media_files/VR
[32] http://www.olcf.ornl.gov/computing-resources/titan-cray-xk7/.

SUPPLEMENTARY INFORMATION

The essential feature of the domain walls imprinted in the experiment [1] is that they can decay via a "snake" instability into vortex rings when the radial extent of the trap becomes larger to the coherence length $R \gg l_{\rm coh}$ [27, 33–35]. The formation of an axially aligned vortex rings from a trapped domain wall is thus almost inevitable: The center of the wall moves faster than the edges so that the wall bows out along the axis of the trap. If the trap is narrow, then the wall maintains integrity (see e.g. Ref. [18]) and one will indeed observe an oscillating domain wall, but as the trap becomes wider, the bowing out will eventually overwhelm the domain wall, establish a circulation, and form a vortex ring. Pinsker *et al.* [36] used this idea to suggest a "piston mechanism" for generating vortex rings, and the MIT experiment [1] essentially reproduces this setup. One thus generically expects a phase imprint to generate vortex rings once the width of the trap exceeds some critical value. The detailed structure of one such a ring from our simulations is down in Fig. 3 shows a cross-section of the cloud.

This behaviour has been studied for bosons (see e.g. [27, 37]), where the transition from a domain wall to a vortex ring appears to be continuous in harmonic tubes (see [27]). Our simulations shown in Fig. 4 suggest that these results also apply qualitatively for fermions. In particular, in the smallest system (left panel of Fig. 4), the vortex ring configuration exists only away from the turning points. It collapses in on itself, re-forming as a domain wall near the turning points and remerges as a vortex ring with an opposite circulation. This behavior mirrors that seen in BEC [26], but is demonstrated here for the first time in a fermionic system. This new domain wall exhibits the same initial instability, and a vortex ring of the opposite circulation and similar size forms and moves back along the trap in the opposite direction. This oscillation is at the limit of the fermionic equivalent of the domain-wall branch of these types of excitations [27]. Note that [27] also discusses collisions of these excitations, which are elastic at low energies. Reducing the width of the trap, one will continuously approach the quasi-1D situation of oscillating domain walls. Note that the period $T \approx \sqrt{3}T_z$ in this case approximately agrees with other the quasi-1D simulations [14, 17, 18]

The motion of a vortex ring in a trapped gas will be modified by the boundary: the outward buoyant force of the trap, for example, will change the axial velocity of the vortex ring according to the well established Magnus relationship. An oscillation can occur whereby a small vortex ring moves along the axis of a trap, primarily according to (1a) and the longitudinal component of the buoyant force, then returns as a larger ring crawling along the edge of the trap (see e.g. [27, 37]). This picture follows from arguments similar to those used to derive (1), but

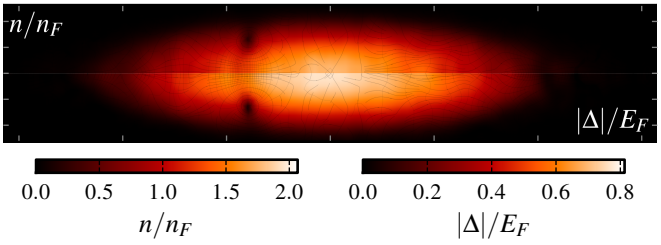

FIG. 3. (color online) The shading (color) contours show slice through the core $x = 0$ the density (top) and magnitude of the order parameter (bottom). Contours of constant phase $\phi = \arg \Delta$ are shown as are streamlines and arrows parallel to the superfluid velocity $\boldsymbol{v} = \boldsymbol{\nabla}\phi$. A higher resolution figure may be found in [31]

where the superflow outside the ring no-longer extends to infinity. As the boundary is reduced, the balance shifts between the opposite flows inside and outside of the ring, slowing, then ultimately reversing the velocity of the ring. A quantitative analysis must include effects such as the entrainment of the surrounding fluid, which can change the effective mass, etc.; see [39] for a few idealized examples. Thus vortex rings can naturally oscillate with periods much larger than T_z in traps where the size of the transverse direction $R \gg 1/k_F$ is large.

TDSLDA Model To demonstrate the generic generation of vortex rings, we simulate the superfluid local density approximation (SLDA) (3) on three 3D lattices of size $24 \times 24 \times 96$, $32 \times 32 \times 128$, and $48 \times 48 \times 128$ with unit lattice spacing. We adjust the particle number — about 230, 560, and 1270 particles for these lattices respectively — so that the density in the core of the initial cylindrical trap [31, 38] corresponds to $k_F = 1$. We evolve about 10^5 wavefunctions in real time using a symplectic split-operator integrator that respects time-reversal invariance using hundreds of GPUs on the Titan supercomputer [32]. Preparing initial states in 3D has been a major challenge for superfluid DFT like the SLDA, but the quantum-friction algorithm introduced in [38] easily overcomes this challenge, and we quickly cool into the ground state of an elongated harmonic trap. As in the experiment, we phase imprint a domain wall, but to reduce phonon noise generated during the imprint, we include a repulsive knife-edge potential. Although the initial conditions have axial symmetry, the simulations here are fully 3D so as not to bias the results.

The simulations evolve a formally infinite system of coupled nonlinear time-dependent PDEs as described in detail elsewhere [13, 29]. The TDSLDA is based on the simplest possible energy density functional that satisfies all expected symmetries. In addition to the number density $n = 2\sum_{E_n<E_c}|v_n|^2$, the Pauli exclusion principle is ensured by including a kinetic density $\tau_c = 2\sum_{E_n<E_c}|\boldsymbol{\nabla} v_n|^2$ in the spirit of the original local density approximation (LDA) introduced by Kohn and Sham [40], and superfluidity is

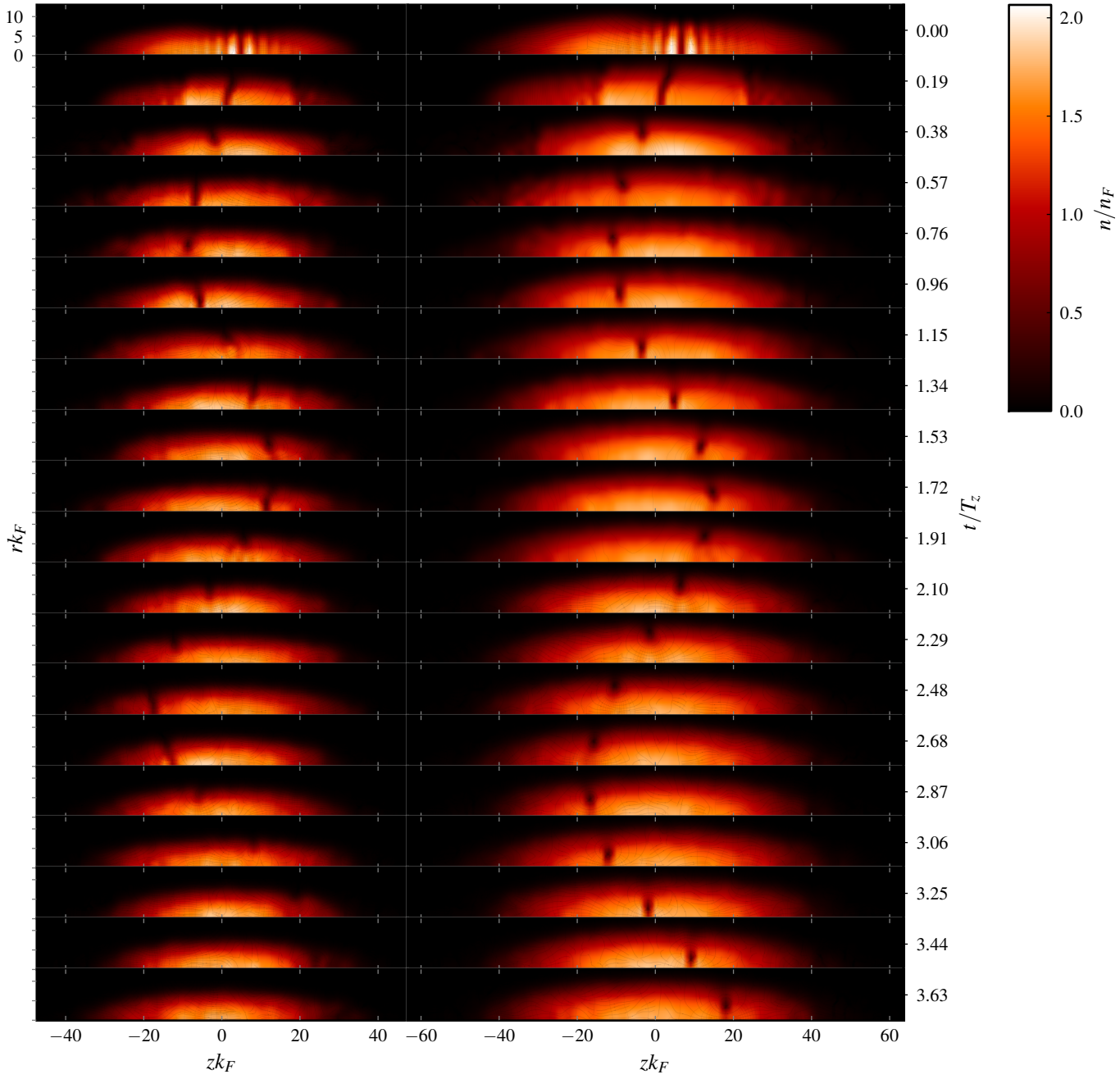

FIG. 4. (color online) Oscillations of a vortex ring in a harmonic trap on a $24 \times 24 \times 96$ lattice (left) and a $32 \times 32 \times 128$ lattice (right). We start with a cylindrical cloud (not shown, see Ref. [31, 38]) with central density $n_F = k_F^3/3\pi^2$ where the Fermi wavevector $k_F = 1/\delta x = 1$. The harmonic trapping potential along z is then increased slowly while applying the quantum cooling algorithm described in [38] to cool the system to a state with two separated clouds. These are the phase imprinted with $\delta\phi = \pi$ and the knife edge is removed, allowing the soliton to evolve as shown. Movies, including a case for a $48 \times 48 \times 128$ lattice, may be found in [31]. This ring then oscillates along the axis of the trap. In the smaller simulation, the ring does not fully form, and it collapses in on itself, re-forming as a dark-soliton near the turning points. This behavior mirrors that seen in BEC [26], but is demonstrated here for the first time in a fermionic system. This new domain wall exhibits the same initial instability, and a vortex ring of the opposite circulation and similar size forms and moves back along the trap in the opposite direction. This oscillation is at the limit of the fermionic equivalent of the domain-wall branch of these types of excitations [27]. Note that [27] also discusses collisions of these excitations, which are elastic at low energies. Reducing the width of the trap, one will continuously approach the quasi-1D situation of oscillating domain walls. Note that the period $T \approx \sqrt{3}T_z$ in this case approximately agrees with other the quasi-1D simulations [14, 17, 18]

modelled by an anomalous density $\nu_c = \sum_{E_n<E_c} v_n^* u_n$. Galilean covariance is restored by including the mass current $\boldsymbol{j} = \frac{\hbar}{m}\sum_{E_n<E_c} 2\,\mathrm{Im}\, v_n \boldsymbol{\nabla} v_n^*$ as discussed in detail in [29, 41]:

$$\mathcal{E} = \frac{\hbar^2}{m}\left[\alpha\frac{\tau_c}{2} - (\alpha-1)\frac{j^2}{2n} + \beta\frac{3(3\pi^2)^{2/3}n^{5/3}}{10} + \right. \\ \left. + \frac{|\nu_c|^2}{n^{1/3}/\gamma + \Lambda_c}\right] + V_{\mathrm{ext}} n, \quad (4)$$

(See Ref. [29] for details on how to express the regulator Λ_c in terms of the energy cutoff E_c.)

The correction to the energy density (4) for $\alpha \neq 1$ is

$$(\alpha-1)\frac{\hbar^2}{2m}\left[\tau_c - \frac{j^2}{n}\right] = (\alpha-1)\frac{\hbar^2}{2m}\left[\tau_c - n v^2\right], \quad (5)$$

where $\boldsymbol{v} = \boldsymbol{j}/n$ is the local velocity. The coefficient $(\alpha-1) \approx 0.1$ in from of τ_c has the effect of slightly softening gradients; the term proportional to j^2 is dominated by phase gradients and vanishes in the ground state where there are no currents $\boldsymbol{j} = 0$. Upon variation ,this correction to the energy density leads to a change in the single-particle Hamiltonian

$$h v_k \to h v_k + (\alpha-1)\left[-\frac{\hbar^2}{2m}\boldsymbol{\nabla}^2 v_k - 2\mathrm{i}\hbar\boldsymbol{v}\cdot\boldsymbol{\nabla} v_k \right. \\ \left. + \left(-\mathrm{i}\hbar\boldsymbol{\nabla}\cdot\boldsymbol{v} + \frac{m\boldsymbol{v}^2}{2}\right) v_k\right]. \quad (6)$$

The gradient term proportional to local velocity $\boldsymbol{v} = \boldsymbol{j}/n$ acts like a gauge potential, and will most affect mostly the flow, barely affecting the density. The last term is a correction to the self-energy of the particle and its magnitude, even close to a vortex core, is very small in the case of a unitary Fermi gas, $\approx 0.1 \times 0.2^2 \varepsilon_F = 0.004\varepsilon_F$, since the maximum value of the velocity around a quantized vortex core is $v \leq 0.2 v_F$ [20].

As with all DFTs, this can be applied to an arbitrary external one-body potential $V_{\mathrm{ext}}(\boldsymbol{x}, t)$. In our first implementation of the time-dependent GPU version of the code we use a split operator method which requires less RAM memory. For this method, gradient terms such as in Eq. (6) are extremely expensive to compute. In our simulations, we use a simpler parameterization with $\alpha = 1$ which avoids the need for the current-dependent term on the second line of (6). This affects the quantitative accuracy of the theory only at the level of a few percent, see also Fig. 5 and the discussion below concerning gradient corrections. The dynamical evolution is described by equations for the quasiparticle wave functions (u_k, v_k)

$$\mathrm{i}\hbar\frac{\partial}{\partial t}\begin{pmatrix} u_k \\ v_k \end{pmatrix} = \begin{pmatrix} h & \Delta \\ \Delta^* & -h \end{pmatrix}\begin{pmatrix} u_k \\ v_k \end{pmatrix}, \quad (7)$$

where the single-particle Hamiltonian h and pairing potential Δ are obtained by taking the appropriate functional derivatives of the energy density $\mathcal{E}$. The dimensionless constants α, β, and γ are fixed by the energy per particle, pairing gap and quasiparticle spectrum obtained from QMC calculations of the homogeneous infinite system. Though Eq. (7) has a similar form as the mean-field BdG equations, it includes a self-energy contribution, which is dominant even at unitarity unlike BdG, and it includes all correlations at the same level of accuracy as the QMC results available so far.

ETF Model To demonstrate the scaling of oscillation periods with system size, aspect ratio, etc. we simulate the ETF model (2) in a cylindrical discrete variable representation (DVR) basis [42] with 2048 points along the z-axis and 256 points in the radial direction, using trapping parameters as described in [1]. We phase imprint a vortex ring with phase $\phi = \arg[z + \mathrm{i}(r - R)]$ ($r = \sqrt{x^2+y^2}$ and R is the vortex ring radius) and "cool" with imaginary time evolution to generate vortex rings with various amounts of background phonon excitations. These are then evolved in real-time using the split-operator integrator to determine the oscillation period, and to perform the rapid-ramp/expansion imaging procedure. Several sample results are shown in Fig. 7, and summarized in the following tables.

The ETF follows from minimizing the energy-density

$$\mathcal{E} = \frac{|\boldsymbol{\nabla}\Psi|^2}{4m} + \mathcal{E}_h(n, a) + V_{\mathrm{ext}} n, \quad (8)$$

where $n = 2|\Psi|^2$ is the total density and we parameterize the equation of state of a dilute Fermi gas for positive scattering lengths with

$$\mathcal{E}_h(n, a) = \frac{3}{5}\varepsilon_F n \xi \frac{\xi + x}{\xi + x(1+\zeta) + 3.0\pi\xi x^2} - \frac{\hbar^2}{2ma^2} n \quad (9)$$

which depends on the magnetic field B through the two-body scattering length a as described in [43, 44] through the dimensionless interaction parameter $x = 1/k_F a$. Dimensions are set in terms of the parameters of the free Fermi gas $n = k_F^3/3\pi^2$, and $\varepsilon_F = \hbar^2 k_F^2/2m$. This reproduces the unitary equation of state with $\xi = 0.370$ and $\zeta = 0.901$ (the contact), and the factor $3.0 = 9a/5a_{DD}$ reproduces the dimer-dimer scattering length $a_{DD} \approx 0.6a$. The ETF approach that has been used to analyze the expansion [28] and [28, 44] breathing mode frequencies of cold atomic gases in a trap, their surface oscillations [45], collisions of clouds of fermions [46], vortex generation [47], vortex pinning [48], and soliton dynamics [49]. The ETF is equivalent to the quantum hydrodynamics approach at zero temperature, which has been used extensively by many authors for modelling the unitary Fermi gas during the last decade, but ETF also includes the quantum pressure term typically neglected in a hydrodynamic approach. We point out that the ETF in Eq. (2) is manifestly covariant under Galilean transformations whereby

$\Psi(\boldsymbol{x},t) \to e^{-2i\phi}\Psi(\boldsymbol{x}+\boldsymbol{v}t,t)$ where $\phi = m\boldsymbol{v}\cdot\boldsymbol{x} + \frac{1}{2}mv^2t$. The factor 2 in the exponent here corresponds with the identification of $\Psi = \langle\psi_a\psi_b\rangle$ as the dimer or di-fermion condensate and could be absorbed into the definition of the dimer mass $m_B = 2m$.

Gradient corrections The SLDA (4) and ETF (8) functionals naturally describe gradients through their kinetic terms, but since they have been fit to properties of homogeneous system, one might reasonably wonder if any significant gradient corrections have been overlooked. This question was addressed in [50] by confronting high-precision QMC calculations of harmonically trapped systems which found that, while small gradient corrections of Weizsäcker-type $\propto -|\boldsymbol{\nabla}n|^2/n$ might improve the ability of the functionals to fit traps with few particles, they can be treated as a perturbative correction to the underlying SLDA (4). Indeed, the SLDA performs extremely well, even when applied to inhomogeneous trapped systems, where it explains virtually all available QMC results for systems with up to 120 fermions, both in polarized and unpolarized systems, in superfluid or normal phases, in harmonic traps, periodic boxes, and infinite matter [29, 30, 51]. This indicates that the kinetic energy density $\tau_c = 2\sum_{E_n<E_c}|\boldsymbol{\nabla}v_n|^2$ properly describes most of the gradient effects. Since the pairing is strong in the unitary Fermi gas, this kinetic energy density includes gradients up to high momenta $\gg k_F$, much larger than the scales $\sim k_F$ describing solitons like domain-walls, vortices, and vortex rings. Thus, though additional gradient corrections may affect the structure of solitons, these effects will be subtle, and will require high-precision QMC calculations and measurements to validate. The omission of these higher-order corrections in our simulations are unlikely to affect our results more than the quoted experimental accuracy, as also illustrated in Fig.5, for a case where density gradients are significant.

The available QMC calculations are not accurate enough to provide a more exact value of the effective mass of the quasi-particles. The QMC results of [52] suggest a value of $\alpha \approx 1.14$ [29] obtained by calculating the ground state energy difference $|E(N\pm1,k) - E(N,0)|$, where N is even and $\hbar k$ is the momentum of the system with $N\pm1$ particles. In that calculation the Bertsch parameter was determined to be $\xi = 0.42(2)$, thus with an error of about 10% when compared to more recent QMC results [53] and experimental measurements $\xi = 0.372$ [44, 54]. One can therefore infer that the error in the quasi-particle dispersion is much larger as it is a difference in energies. The QMC calculation [52] for the pairing gap quotes an error of about 5% ($\Delta = 0.504(24)\varepsilon_F$). This agrees within the error bars with an independent analysis of experimental data of polarized system [55], which claims that $\Delta = 0.45(5)\varepsilon_F$. In an independent QMC study at finite temperatures [56], the effective mass was found to be consistent with the bare mass to within 10% for a large range of temperatures. In summary, all direct information from QMC calculations and experiments contain errors at the level of about 10%, statistical as well systematic, consistent with $\alpha - 1 \leq 0.1$.

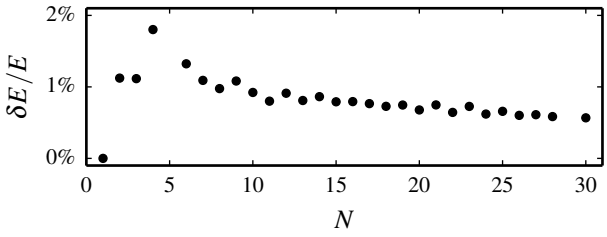

FIG. 5. (color online) Relative energy change (in %) between simulations with $\alpha = 1$ and $\alpha = 1.14$ that compute the energy of N fermions (both even and odd particle numbers) in the unitary Fermi gas trapped in an isotropic harmonic oscillator. The parameters β and γ for the SLDA here have been adjusted to match the values of ξ and η used in Ref. [29] for fixed $\alpha = 1.14$ and $\alpha = 1.00$. This demonstrates that a 14% change in α results in less than 2% change in energies, even in very small systems which have relatively large gradients. The use of the bare mass in DFT calculations is in the spirit of original Hohenberg and Kohn and Kohn and Sham formulation, which is widely used in electronic calculations in condensed matter physics and chemistry.

Results The results of the expansion and imaging process are shown in Fig. 2 and Fig. 6 (see [31] for movies). Here it becomes clear why the experiment [1] needed to implement an involved ramping/imaging procedure to image the defects. The rapid ramp into the BEC regime at low magnetic fields $B_{\rm min} < 700$ G causes a rapid change in the coherence length that produces a sort of shock-wave during the expansion. The geometry to the expansion results in an asymmetric density depletion that resolves into a planar looking object when imaged with the coarse-grain resolution of the imaging system. If the field $B_{\rm min}$ not sufficiently small, then the shock-wave is mild, and the resulting cloud does not have enough contrast to register a signal. That the ETF quantitatively reproduces the required minimum field $B_{\rm min}$ is further validation of the DFT and somewhat expected since the ETF approximation should become more accurate in the BEC regime.

The ETF certainly cannot reproduce all details of the fermionic dynamics – in particular, one expects poor behavior when excitations approach the pair-breaking threshold set by the gap $\hbar\omega > 2\Delta \approx E_F$. The theory, however, has the same symmetries, and is tuned to have the same equation of state as the full theory. The advantage of this approach over traditional fermionic time-dependent density functional theorys (TDDFTs) is its computational simplicity: the bosonic approach needs only to evolve a single wavefunction. A detailed comparison of the ETF and SLDA is performed in [57].

In Table I we compared the oscillation periods predicted by the ETF with the observed period from [1] on resonance

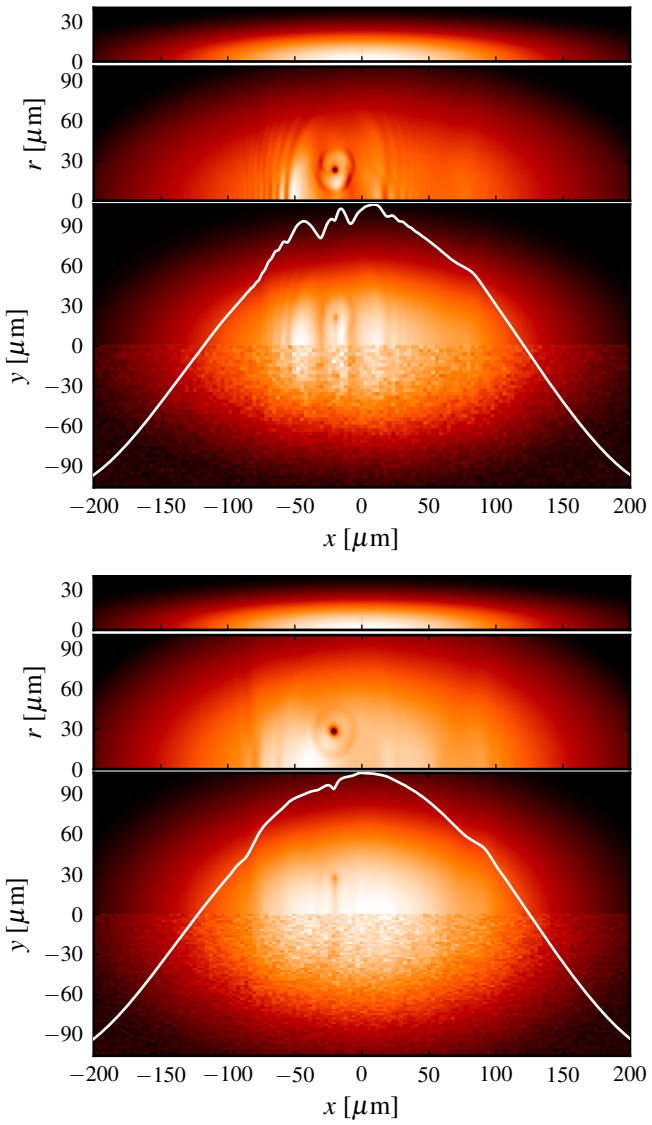

FIG. 6. (color online) Additional expansion images with same interpretation as in Fig. 2. Top: image of a small vortex ring expanded at $B_{\rm min} = 580$ G. Bottom: image of same small vortex ring expanded at $B_{\rm min} = 702$ G demonstrating that $B_{\rm min} < 700$ G is required to achieve a resolvable image, thereby explaining the need for the subtle time-of-flight expansion and imaging procedure discussed in the experiment [1]. See [31] for movies.

for the three aspect ratios studied in the experiment. The observations are consistently larger than the ETF predictions by a factor of about 1.8: this might be due to the lack of a normal component filling the core of the vortices in the ETF and is reminiscent of the factor $\sqrt{3/2}$ difference in the calculated period of 1D domain walls. This is consistent with the heuristic estimate (1b) whereby the mass depletion M_{VR} would be suppressed for fermions by the presence of the normal state.

To test the consistency of this suppression, we use the ETF to model the TDSLDA simulations shown in Fig. 4. The comparison is shown in Table II where it is seen that the TDSLDA periods are larger than the ETF by a factor consistent with $\sqrt{3/2}$ for small systems. This is expected since these simulations are in small traps and are very close to the limit where domain walls remain stable. The lattice simulation $48 \times 48 \times 128$, which involved 259 762 complex time-dependent 3D nonlinear coupled partial differential equations, performed on Titan [32] on 2048 GPUs, is one of the largest Direct Numerical Simulations (DNC) performed so far.

TABLE II. Benchmark of the ETF periods to the SLDA periods for sizes $24 \times 24 \times 96$, $32 \times 32 \times 128$, and $48 \times 48 \times 128$.

Size	$T_{\rm ETF}$	$T_{\rm SLDA}$	$T_{\rm SLDA}/T_{\rm ETF}$
$24 \times 24 \times 96$	$1.4T_z$	$1.7T_z$	1.2
$32 \times 32 \times 128$	$1.6T_z$	$1.9T_z$	1.2
$48 \times 48 \times 128$	$1.9T_z$	$2.6T_z$	1.4

In Table III we demonstrate how the period depends on the initial radius of the imprinted vortex ring R_0. This parameter is not directly measured or controlled in the experiment, so we must estimate the value $R_0 \approx 0.2R_\perp$ by the resulting amplitude of oscillation $\sim 0.5R_z$ shown in the figures of [1].

TABLE III. Imprinting the vortex with different radii, all on resonance with $1/\lambda = 3.3$. In the tables below we show how oscillation period changes with aspect ratio for a vortex ring imprinted at $R_0 = 0.30\ R_\perp$ on resosnace $k_F a = \infty$ in each scenario.

Imprint radius	Period	Amplitude
$R_0 = 0.20\ R_\perp$	$T = 8.6\ T_z$	$\sim 0.45\ R_z$
$R_0 = 0.30\ R_\perp$	$T = 9.9\ T_z$	$\sim 0.35\ R_z$
$R_0 = 0.40\ R_\perp$	$T = 10.7\ T_z$	$\sim 0.15\ R_z$
$R_0 = 0.50\ R_\perp$	$T = 11.0\ T_z$	$\sim 0.05\ R_z$

Finally, we comment on the observed "snake" instability discussed in the supplementary information of [1]. Although significantly more stable than domain walls, large vortex rings can also bend and decay through the Crow instability [58, 59] and the MIT experiment is poised right on the edge of the regime where one can start to explore the quantum turbulence cascade.

[33] B. P. Anderson, P. C. Haljan, C. A. Regal, D. L. Feder, L. A. Collins, C. W. Clark, and E. A. Cornell, Phys. Rev. Lett. **86**, 2926 (2001), arXiv:cond-mat/0012444v1.
[34] J. Brand and W. P. Reinhardt, Phys. Rev. A **65**, 043612 (2002), arXiv:cond-mat/0105581 [cond-mat.soft].
[35] N. G. Berloff, Phys. Rev. B **65**, 174518 (2002), arXiv:cond-mat/0107148 [cond-mat.soft].

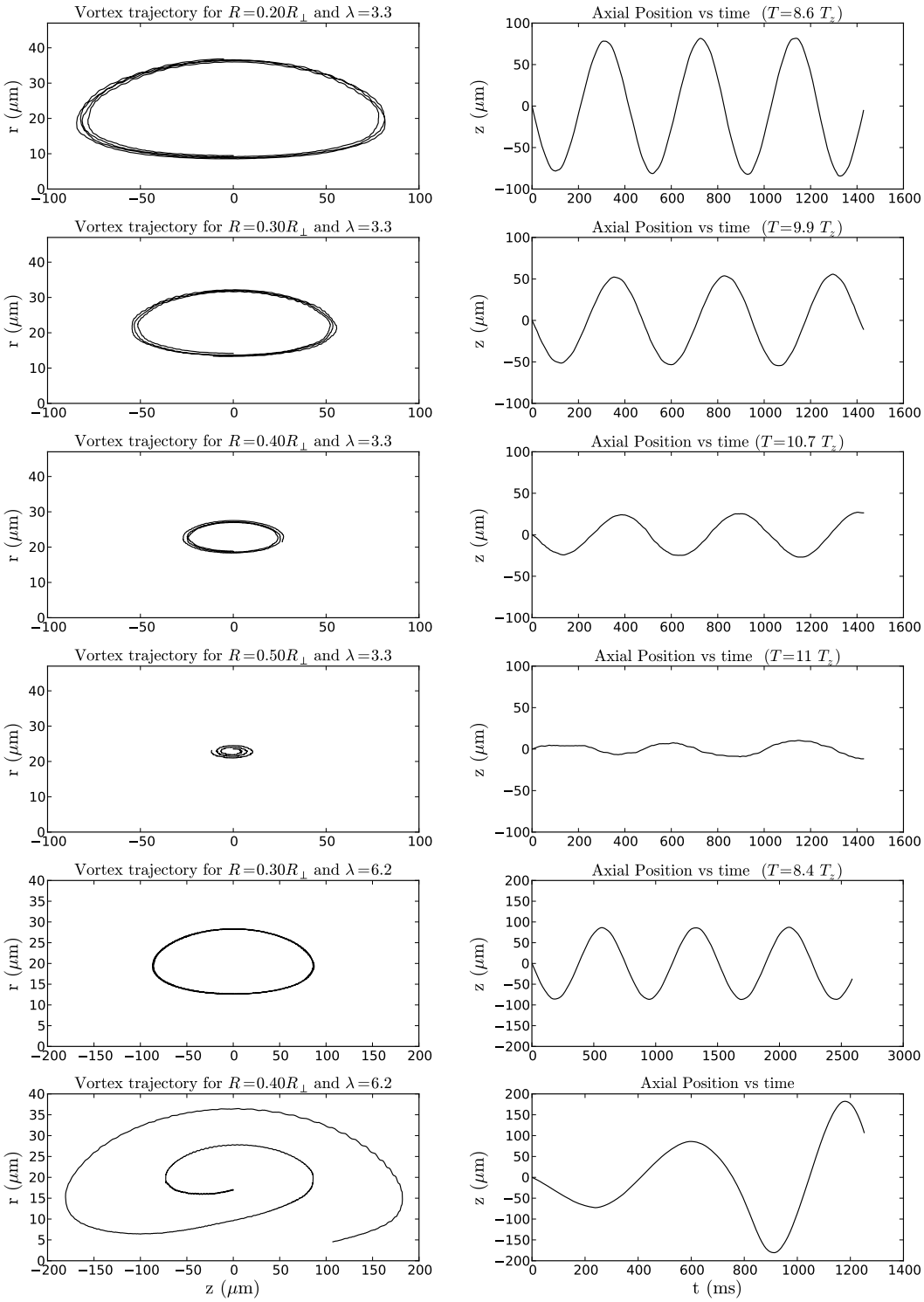

FIG. 7. Left column shows various trajectories of a vortex ring in the R-z–plane, while the right column shows the time dependence of corresponding z-coordinate of the vortex ring. The forth row show an example of an almost stationary vortex ring. The radius of a stationary vortex ring is $\approx 0.49R_\perp$, where $R_\perp$ is the TF radius of the cloud. The last row shows an example of a vortex ring trajectory in the presence of a considerable number of phonons.

[36] F. Pinsker, N. G. Berloff, and V. M. Pérez-García, "Nonlinear quantum piston for the controlled generation of vortex rings and soliton trains," (2013), arXiv:1305.4097 [cond-mat.quant-gas].

[37] T. W. Neely, E. C. Samson, A. S. Bradley, M. J. Davis, and B. P. Anderson, Phys. Rev. Lett. **104**, 160401 (2010), arXiv:0912.3773 [cond-mat.quant-gas]; P. Engels, Physics **3**, 33 (2010).

[38] A. Bulgac, M. M. Forbes, K. J. Roche, and G. Wlazłowski, "Quantum Friction: Cooling Quantum Systems with Unitary Time Evolution," (2013), arXiv:1305.6891 [nucl-th].

[39] P. Magierski and A. Bulgac, Acta Phys. Pol. B **35**, 1203 (2004), arXiv:astro-ph/0312644.

[40] W. Kohn and L. J. Sham, Phys. Rev. **140**, A1133 (1965).

[41] Y. M. Engel, D. M. Brink, K. Goeke, S. J. Krieger, and D. Vautherin, Nucl. Phys. A **249**, 215 (1975).

[42] R. G. Littlejohn and M. Cargo, J. Chem. Phys. **117**, 27 (2002).

[43] M. Bartenstein, A. Altmeyer, S. Riedl, R. Geursen, S. Jochim, C. Chin, J. H. Denschlag, R. Grimm, A. Simoni, E. Tiesinga, C. J. Williams, and P. S. Julienne, Phys. Rev. Lett. **94**, 103201 (2005), arXiv:cond-mat/0408673.

[44] G. Zürn, T. Lompe, A. N. Wenz, S. Jochim, P. S. Julienne, and J. M. Hutson, Phys. Rev. Lett. **110**, 135301 (2013), arXiv:1211.1512; Y. E. Kim and A. L. Zubarev, Phys. Rev. A **72**, 011603 (2005), arXiv:cond-mat/0502651; J. Phys. B **38**, Jul. (2005), arXiv:cond-mat/0505139.

[45] L. Salasnich, F. Ancilotto, and F. Toigo, Laser Phys. Lett. **7**, 78 (2010), arXiv:0909.2344; L. Salasnich, Few-Body Sys. **54**, 697 (2013), arXiv:1204.1659.

[46] F. Ancilotto, L. Salasnich, and F. Toigo, Phys. Rev. A **85**, 063612 (2012), arXiv:1206.0568; J. Low Temp. Phys. , 471 (2012), arXiv:1210.2437.

[47] F. Ancilotto, L. Salasnich, and F. Toigo, Phys. Rev. A **87**, 013637 (2013), arXiv:1301.5133 [cond-mat.quant-gas].

[48] A. Bulgac, M. M. Forbes, and R. Sharma, Phys. Rev. Lett. **110**, 241102 (2013), arXiv:1302.2172 [nucl-th].

[49] A. Khan and P. K. Panigrahi, "Bell Soliton in Ultracold Atomic Fermi Gas," (2013), arXiv:1304.3579 [cond-mat.quant-gas].

[50] M. M. Forbes, submitted to Phys. Rev. (2013), arXiv:1211.3779 [cond-mat.quant-gas].

[51] M. M. Forbes, S. Gandolfi, and A. Gezerlis, Phys. Rev. Lett. **106**, 235303 (2011), arXiv:1011.2197 [cond-mat.quant-gas].

[52] J. Carlson and S. Reddy, Phys. Rev. Lett. **95**, 060401 (2005), arXiv:cond-mat/0503256.

[53] J. Carlson, S. Gandolfi, K. E. Schmidt, and S. Zhang, Phys. Rev. A **84**, 061602 (2011), arXiv:1107.5848.

[54] M. J. H. Ku, A. T. Sommer, L. W. Cheuk, and M. W. Zwierlein, Science **335**, 563 (2012), arXiv:1110.3309.

[55] J. Carlson and S. Reddy, Phys. Rev. Lett. **100**, 150403 (2008), arXiv:0711.0414 [cond-mat].

[56] P. Magierski, G. Wlazłowski, A. Bulgac, and J. E. Drut, Phys. Rev. Lett. **103**, 210403 (2009).

[57] M. M. Forbes and R. Sharma, "Validating simple dynamical simulations of the unitary fermi gas," arXiv:1308.4387 [cond-mat.quant-gas].

[58] S. C. Crow, *AIAA Journal*, AIAA Journal **8**, 2172 (1970).

[59] S. Gautam, Mod. Phys. Lett. **B27**, 1350097 (2013), arXiv:1206.1825 [cond-mat.quant-gas].